

Quantum dynamics of instability-induced pulsations of a Bose-Einstein condensate in an optical lattice

Uttam Shrestha,¹ Juha Javanainen,¹ and Janne Ruostekoski²

¹*Department of Physics, University of Connecticut, Storrs, CT 06269-3046*

²*School of Mathematics, University of Southampton, Southampton, SO17 1BJ, UK*

(Dated: January 22, 2009)

We study the dynamics of a Bose-Einstein condensate in a one-dimensional optical lattice in the limit of weak atom-atom interactions, including an approximate model for quantum fluctuations. A pulsating dynamical instability in which atoms periodically collect together and subsequently disperse back into the initial homogeneous state may occur in the time evolution. We take into account the quantum fluctuations within the truncated Wigner approximation. We observe that the quasiperiodic behavior still persists for a single realization that represents a typical experimental outcome, but ensemble averages show various manifestations of quantum fluctuations. Quantum effects become more prominent when the effective interaction strength is increased.

PACS numbers: 03.75.Lm, 03.75.Kk

I. INTRODUCTION

The superfluidity of a Bose-Einstein condensate (BEC) in an optical lattice has been drawing considerable attention in the last several years [1]. As is well known, superflow of the BEC in free space suffers from an instability when the flow velocity reaches a critical value. Such an instability, known as Landau or energetic instability, exists when the superfluid flow is not a local minimum of energy and the system may lower its energy by emitting phonons [2]. In an optical lattice, in addition to energetic instability, the BEC may also exhibit dynamical or modulational instabilities that have been the subject of much experimental and theoretical research over recent years [3, 4, 5, 6, 7, 8, 9, 10, 11, 12, 13, 14, 15, 16, 17, 18, 19, 20]. When the system is in the dynamically unstable regime, small perturbations grow exponentially in time resulting in irregular dynamics, loss of coherence, or an abrupt stop of the transport of the atom cloud [4, 5].

In this paper we study dynamical instabilities of atoms in an optical lattice for the case of weak atom-atom interactions and also taking into account quantum fluctuations of the atoms. We recently reported [20] that, by appropriately selecting the strength of the atom-atom interactions, the corresponding classical system may exhibit a pulsating dynamical instability in which the atoms nearly periodically collect to a peak in lattice occupation numbers, and subsequently disperse back to (very close to) the initial unstable state. This is different from the conventional view, valid at strong interatomic interactions, that dynamical instabilities for BECs in optical lattices are associated with irregular dynamics. The dynamics of an integrable double-well system provides a qualitative explanation of the pulsating phenomenon [20]: Although the instability is a result of the interplay between the lattice discreteness and the nonlinearity that makes the lattice non-integrable, the dynamics of the lattice with many sites approximates the dynamics of an integrable system. Related classical pulsations starting

from already compressed atom distribution in a lattice have been discussed in [18] within the framework of the nonpolynomial Schrödinger equation.

As the emergence of dynamical instabilities can also be closely related to various fundamental effects in nonequilibrium quantum dynamics, for example dissipative transport [15] and quantum phase transitions [21], it is particularly interesting to address how an entirely classical description of the pulsating instability [20], embodied in the Discrete Nonlinear Schrödinger equation (DNLSE), is modified as a result of quantum fluctuations. In this paper we provide an approximate analysis of the quantum effects on the pulsating instability, as well as amend the discussion of Ref. [20] with additional details and angles.

We consider different dynamically stable initial stationary superfluid flow states that are instantaneously transferred to a dynamically unstable regime by changing the strength of atom-atom interactions. We incorporate quantum fluctuations of the atoms using a stochastic phase-space method, the Truncated Wigner Approximation (TWA), [22, 23, 24, 25, 26]. We find that the quasiperiodic behavior is still observable in individual stochastic realizations that represent typical outcomes of individual experiments. In fact, the damping of the quasiperiodic pulsating instability in a single stochastic trajectory remains very weak even in the presence of enhanced quantum fluctuations and for the case of an initial state with a substantial noncondensate atom fraction. However, as the timing, shape and location of the pulsation events in each realization change due to quantum effects, in the quantum mechanical ensemble average the wave function revival become progressively weaker, with an increased damping rate, when the effective interaction strength is increased. Other ensemble averages provide additional quantitative information about the effects of quantum fluctuations. For instance, in the limit of weak quantum fluctuations, the amplitude of the pulsating instability approaches the classical value obtainable from the DNSLE with a weak random noise seeding the insta-

bility, but for enhanced quantum fluctuations both the amplitude and the amplitude fluctuations of the pulsations become significantly larger than in the classical system.

In Sec. II we formulate the theoretical model, mainly the Gross-Pitaevskii equation (GPE) [27] and its discrete variant, the DNLS [5, 28]. We use linear stability analysis to find the region of interaction strengths and flow quasimomenta where the system develops an instability. In Sec. III we investigate the time evolution of the DNLS, i.e., classical mean-field theory. Although the system initially develops an instability, the subsequent time evolution shows nearly periodic recurrence to the initial state. In Sec. IV we review the well understood double well system and argue that the dynamical behavior of the multi-site system is analogous to the two-site system, at least in the limit of weak nonlinearity. In Sec. V we study the dynamics beyond the classical mean field theory using the TWA. We compare various physical properties such as the number fluctuations and the overlaps of the state of the system in single realizations with an ensemble averages in a few quantitative examples. The basic phenomenon of pulsations survive quantum corrections, but substantial modifications to the classical picture emerge when the atom number is reduced while keeping the chemical potential fixed.

II. THEORETICAL MODEL: DNLS

At zero temperature the dynamics of a weakly interacting BEC in an optical lattice can be modeled by the mean field Gross-Pitaevskii equation [2, 27]

$$i\hbar \frac{d\Psi}{dt} = \left(-\frac{\hbar^2}{2m} \Delta + V(\mathbf{x}) + g_3 |\Psi|^2 \right) \Psi, \quad (1)$$

where $\Psi(\mathbf{x}, t)$ is a wave function corresponding to the bosonic field operator such that $|\Psi(\mathbf{x})|^2 = n(\mathbf{x})$ equals the atom density. The coupling constant g_3 is related to the scattering length through $g_3 = 4\pi\hbar^2 a/m$, where a and m are the s -wave scattering length and atomic mass. The positive and negative scattering lengths respectively correspond to the repulsive and attractive atom-atom interactions. The Eq. (1) is an approximate description of an assembly of a large number of bosonic atoms that are in the same quantum mechanical state. Since the equation is nonlinear, the coefficient g_3 depends on the normalization of the wave function. Here the wave function is normalized to atom number N , so that we have

$$\int d^3x |\Psi(\mathbf{x})|^2 = N. \quad (2)$$

The GPE is an increasingly accurate approximation to the underlying quantum field theory, for instance, in the formal limit $N \rightarrow \infty$, $g_3 \rightarrow 0$ with Ng_3 and the system volume held constant.

We consider the external potential, $V(\mathbf{x})$, of the form

$$V(\mathbf{x}) = \frac{1}{2}m(\omega_x^2 x^2 + \omega_\perp^2 r_\perp^2) + V_0 \sin^2\left(\frac{\pi x}{d_L}\right). \quad (3)$$

Here V_0 and $d_L (= \lambda/2)$ are the depth and the periodicity of the optical lattice. If the harmonic confinement is much stronger in the transverse than in the longitudinal direction ($\omega_\perp \gg \omega_x$) the GPE can be transformed into a one-dimensional form

$$i\hbar \frac{d\psi}{dt} = \left(-\frac{\hbar^2}{2m} \frac{\partial^2}{\partial x^2} + V(x) + g_1 |\psi|^2 \right) \psi, \quad (4)$$

with an effective atom-atom interactions $g_1 = 2a\hbar\omega_\perp$. Furthermore, when the depth of the optical lattice is much larger than the chemical potential of the atoms, one can employ the tight-binding approximation. By expressing the condensate wave function $\psi(x)$ as a superposition of Wannier functions localized within each potential well of the lattice, one may obtain the tight-binding version of the GPE known as the discrete nonlinear Schrödinger equation (DNLS) [5],

$$i\frac{\partial}{\partial t}\psi_l = -J(\psi_{l+1} + \psi_{l-1}) + (V_l + \chi |\psi_l|^2)\psi_l. \quad (5)$$

We employ periodic boundary conditions. This means that for L lattice sites numbered as $l = 0, 1, \dots, L-1$, the sites $l = L$ actually refers to the site $l = 0$ and $l = -1$ to the site $l = L$. Physically this corresponds to a ring lattice. For other types of boundary conditions there obviously have to be some changes in the results. For instance, in case of hard-wall boundary conditions a state of the atoms that would propagate around a ring will instead reflect back from the ends of the lattice. However, such variations of the theme will not be discussed further in this paper.

The parameters J and V_l characterize the tunneling rate of the atoms from site to site and the external trapping potential, respectively, whereas χ is proportional to the atom-atom interactions. Henceforth we ignore the non-lattice potential in the direction of the lattice, and correspondingly set $V_l \equiv 0$. The value of the interaction parameter χ depends on the normalization of the wave function, i.e., of the complex numbers ψ_l ,

$$\mathcal{N} = \sum_l |\psi_l|^2. \quad (6)$$

Differently from both the GPE (1) and Ref. [20], here we normalize the state to the one, $\mathcal{N} = 1$. Even though the numbers $|\psi_l|^2$ then equal the fractions of the atoms residing at the sites l , in what follows we nonetheless call them populations, or downright atoms numbers. The interaction coefficient is expressed in terms of the (actually three-dimensional) unit-normalized wave function of an atom in one (actually three-dimensional) potential well of the lattice $w(\mathbf{x})$ as

$$g = \frac{4\pi\hbar a}{m} \int d^3x |w(\mathbf{x})|^4, \quad \chi = \frac{N}{L}g, \quad (7)$$

which explicitly shows the difference between the inherently atomic coupling constant, g , and the coupling constant appearing in the DNLS, χ . We frequently regard the atomic coupling g as variable, which might be achieved by employing a Feshbach resonance. The DNLS becomes increasingly accurate, for instance, in the asymptotic limit $N \rightarrow \infty$ with χ and L held constants. Unless it is explicitly stated otherwise, we assume here that $J > 0$ and the atom-atom interaction is repulsive, $\chi \geq 0$.

In the absence of the remnant trapping potential and nonlinearity Eq. (5) may be solved with a plane-wave ansatz

$$\psi_l^0(t) = \sqrt{\frac{1}{L}} e^{i[p l - \omega(p)t]}, \quad (8)$$

giving the dispersion relation

$$\omega(p) = -2J \cos p. \quad (9)$$

The boundary conditions quantize the lattice momentum p to the values

$$p = \frac{2\pi}{L} P \quad (10)$$

where P is an integer that may be chosen to lie in the interval $[-\frac{L}{2}, \frac{L}{2})$. For notational convenience we always take the number of lattice sites L to be even.

When the interaction is switched on, the constant-amplitude plane waves are still stationary solutions to Eq. (5) but with a modified dispersion relation

$$\omega(p) = -2J \cos p + \frac{\chi}{L}. \quad (11)$$

Besides these extended-wave solutions, the nonlinear system may also admit stationary solutions, of the form $\psi_l(t) = \psi_l(0)e^{-i\mu t}$, which are localized in space [29]. These solutions, so-called gap solitons, usually have an energy that lies outside of the linear band spectrum. In the continuum model solitonic solutions of the nonlinear Schrödinger equation can be found in closed form by using the inverse scattering method [30]. However, the discrete system has fewer constants of the motion and is not integrable as such, so that one has to rely on numerical techniques for exact solutions.

A. Modulational instability

To study the stability of a the plane wave solution (8) and (11), we introduce a perturbation around the steady state [4, 5],

$$\psi_l(t) = \psi_l^0(t)[1 + u_q e^{i(q l - \Omega_q t)} + v_q^* e^{-i(q l - \Omega_q^* t)}], \quad (12)$$

where q and Ω_q are the quasimomentum and the frequency of the small excitation relative to the initial unperturbed steady state, and u_q, v_q are assumedly small

mode amplitudes. By the periodic boundary conditions the possible excitation modes q are also quantized and may be characterized by an integer $Q \in [-L/2, L/2)$, so that

$$q = \frac{2\pi Q}{L}. \quad (13)$$

$Q = 0$, though, corresponds to a change in the normalization of the unperturbed state ψ_l^0 , and does not qualify as an excitation.

After inserting Eq. (12) in Eq. (5) with $V_l = 0$, and expanding to the lowest nontrivial order in u_q and v_q we get the following matrix equation,

$$i \frac{dU_q}{dt} = \mathcal{M} U_q, \quad (14)$$

where U_q is the vector $[u_q, v_q]^T$ and \mathcal{M} is a 2×2 matrix with the elements

$$\begin{aligned} \mathcal{M}_{11} &= \frac{\chi}{L} + 4J \sin \frac{q}{2} \sin(\frac{q}{2} + p), \\ \mathcal{M}_{22} &= -\frac{\chi}{L} - 4J \sin \frac{q}{2} \sin(\frac{q}{2} - p), \\ \mathcal{M}_{12} &= -\mathcal{M}_{21}^q = \frac{\chi}{L}. \end{aligned} \quad (15)$$

The eigenvalues of \mathcal{M} give the small-excitation frequencies,

$$\Omega_q = 2J \sin p \sin q \pm \Gamma_q; \quad (16)$$

$$\Gamma_q = \sqrt{J \cos p \sin^2 \frac{q}{2} \left[2J \cos(p) \sin^2 \frac{q}{2} + \frac{\chi}{L} \right]}, \quad (17)$$

whereas the eigenvectors give the corresponding mode amplitudes,

$$u_q = \sqrt{\frac{4J \cos p \sin^2 \frac{q}{2} \pm \Gamma_q + \frac{\chi}{L}}{2\Gamma_q}}, \quad (18)$$

$$v_q = \sqrt{\frac{4J \cos p \sin^2 \frac{q}{2} \mp \Gamma_q + \frac{\chi}{L}}{2\Gamma_q}}. \quad (19)$$

As long as the quantity Γ_q , Eq. (17) is real, the frequency of the excitation mode Ω_q is also real and the amplitudes u_q and v_q are chosen to satisfy the normalization conditions $|u_q|^2 - |v_q|^2 = \pm 1$, the sign depending on the mode. The reason for this normalization is that in quantum theory a unit-normalized state

$$\psi_l(p, q) = \frac{1}{\sqrt{L}} (u_q e^{i(p+q)l} + v_q^* e^{i(p-q)l}) \quad (20)$$

then represents one bosonic elementary excitation of the condensate. There are two excitation modes corresponding to the \pm signs in Eqs. (16)-(19) for each quasimomentum q , but only those with positive normalization

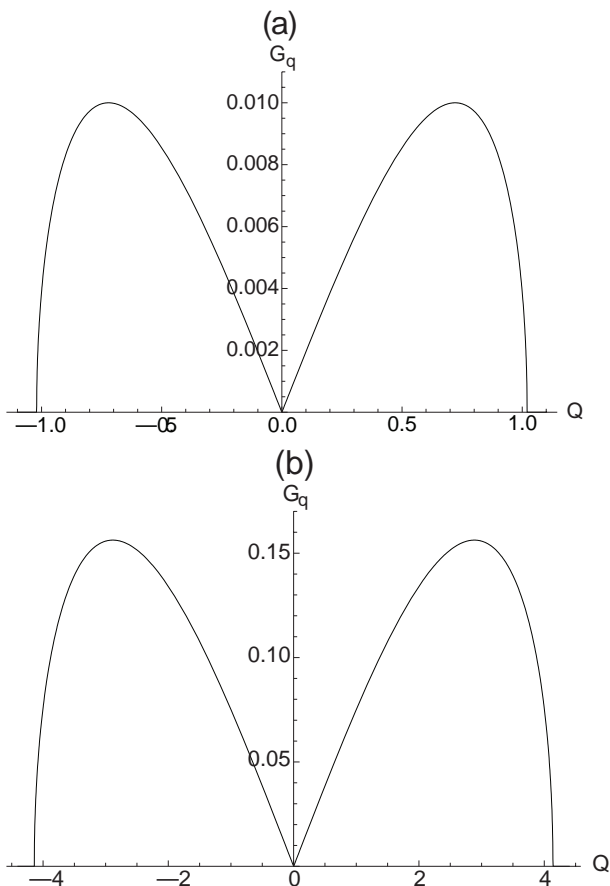


FIG. 1: Coefficient of exponential gain G_q for an excitation mode as a function of the parameter Q related to quasimomentum q by $Q = Lq/(2\pi)$. The parameters characterizing the interaction strength are $\Lambda = 0.32$ (a) and $\Lambda = 5.0$ (b). Modulational instability is only possible for $G_q > 0$, and excitation modes may only occur at nonzero integer values Q .

give physical small-excitation modes. The modes corresponding to negative normalization are artifacts of the present Bogoliubov type analysis, and are henceforth ignored. For more details on the linear stability analysis and its relation to quantum field theory consult, e.g., Refs. [31, 32].

Since we are dealing with the repulsive atom-atom interactions, $\chi \geq 0$, all small-excitation frequencies Ω_q are real for $|p| \leq \pi/2$. However, the existence of complex eigenvalues cannot be ruled out in the interval $|p| \in (\frac{\pi}{2}, \pi]$, depending on the values of J , χ , q and p . If for a given p there exists a mode q such that the quantity Γ_q is imaginary, there is a small excitation that grows exponentially. This signals a dynamical instability of the steady-flow mode p . For a dynamically unstable excitation mode q we have $|u_q|^2 - |v_q|^2 \equiv 0$, so that unstable modes cannot be normalized to one [4].

Figure 1 shows the gain coefficient,

$$G_q = \frac{|\Im \Omega_q|}{2J}, \quad (21)$$

for two cases (a) $\Lambda = 0.32$, and (b) $\Lambda = 5.0$, where the dimensionless interaction strength Λ is defined to be

$$\Lambda = \frac{\chi}{2J}. \quad (22)$$

Here we consider a lattice with $L = 32$ sites for $p = \pi$. Figure 1(a) reveals a single pair of unstable mode with $Q = \pm 1$, whereas Fig. 1(b) shows four pairs of unstable modes.

Analytically, for any $|p|$ greater than $\pi/2$ and in the limit of large L , the eigenfrequency for the excitation mode Q will be complex if

$$\Lambda > |\cos(p)| \frac{\pi^2 Q^2}{L}. \quad (23)$$

The corresponding expression for the gain coefficient is

$$G_q = \frac{2\pi Q \sqrt{|\cos p| (L\Lambda - \pi^2 Q^2 |\cos p|)}}{L^2}, \quad (24)$$

and the characteristic time scale for the dynamical instability τ_q is given by

$$2J\tau_q = \frac{1}{G_q}. \quad (25)$$

The flow with the quasimomentum p is dynamically unstable if the inequality (23) is true at least for the longest-wavelength excitation with $Q = 1$. The critical interaction strength approaches zero when the number of lattice sites L tends to infinity, whether for a fixed atom number or if the atom density $\propto N/L$ is held constant. In this way any flow with $|p| > \pi/2$ will turn unstable with $L \rightarrow \infty$. The imaginary part of the complex eigenfrequency as well as the corresponding eigenvectors are the same for the modes Q and $-Q$ [see Eqs. (18), (19)], so that we regard these two modes as equivalent as it comes to the instability.

III. TIME EVOLUTION AND PULSATING INSTABILITY

We carry out numerical simulations on the DNLSE to study the growth of the unstable excitation mode in a lattice for a suitable range of interaction parameters. For a given number of lattice sites L and flow momentum p , the number of unstable modes in the linear stability analysis depends only on the interaction parameter Λ , Eq. (22). Here we focus on long-wavelength excitations in the limit of weak atom-atom interactions. Two numerical methods have been used for the time evolution, an unconditionally stable Crank-Nicholson type algorithm [33] and a sixth-order accurate FFT split operator algorithm that works in the same way for DNLSE as is discussed in Ref. [34] with the ordinary GPE.

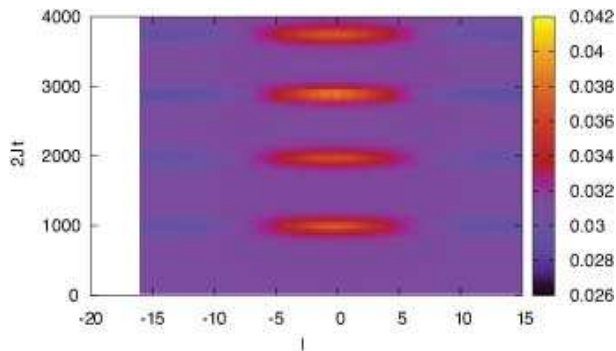


FIG. 2: (Color online) Collapse and revival of the density pulse in the BEC evolution when the lattice starts from a dynamically unstable state in a density plot for the populations of the sites $|\psi_l|^2$, the lighter shades corresponding to larger populations. The parameters are $\Lambda = 0.48$, $p = \pi$, and $L = 32$. These parameters correspond to a single unstable mode, as per linear stability analysis. The instability drives the initial homogeneous atom distributions into a density peak that subsequently disperses back to the initial state, and the process repeats.

A. Single unstable mode

A perusal of the condition (23) shows that the range of interaction strengths where the $Q = 1$ mode is unstable but the $Q = 2$ mode is not is given by

$$|\cos p| \frac{\pi^2}{L} < \Lambda \leq 4|\cos p| \frac{\pi^2}{L}. \quad (26)$$

Figure 2 shows a typical density plot of the time evolution of the BEC initially prepared in the plane wave state at the edge of the Brillouin zone ($p = \pi$) seeded with random Gaussian noise, for the number of lattice sites $L = 32$ and the interaction strength $\Lambda = 0.48$. This value of Λ corresponds to one unstable mode in the linear stability analysis. Although a tiniest amount of noise (either in real experiments or in numerical simulations) is sufficient to trigger the instability, an external noise of amplitude $\sim 10^{-4}$ is added to speed it up. The same applies to all of our demonstrations of the pulsating instability in multisite lattices up to Sec. V, where we adopt a model for the quantum noise instead. It has been tested in a number of runs that the time for the onset of the instability for fixed values of the other parameters depends logarithmically on the amplitude of the added noise, as it should.

Figure 3 depicts snapshots of a pulse that moves during its formation from the initial flow state with quasi-momentum $p = 15\pi/16$. In this figure we take a larger lattice with $L = 128$ sites and the interaction strength is $\Lambda = 0.25$, so that there is still one and only one unstable mode. The pulsating behavior of the peak still persists but the peak moves. By virtue of the periodic boundary conditions a pulse that goes over the right edge will reappear at the left edge of the lattice.

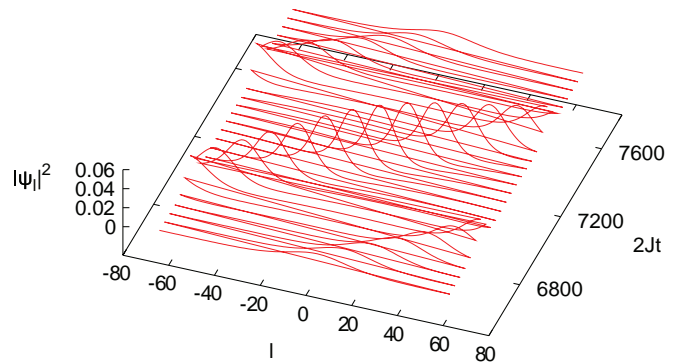


FIG. 3: (Color online) Density evolution of the BEC for the initial flow momentum different from π . Here the parameters are $L = 128$, $\Lambda = 0.25$ and $p = 15\pi/16$.

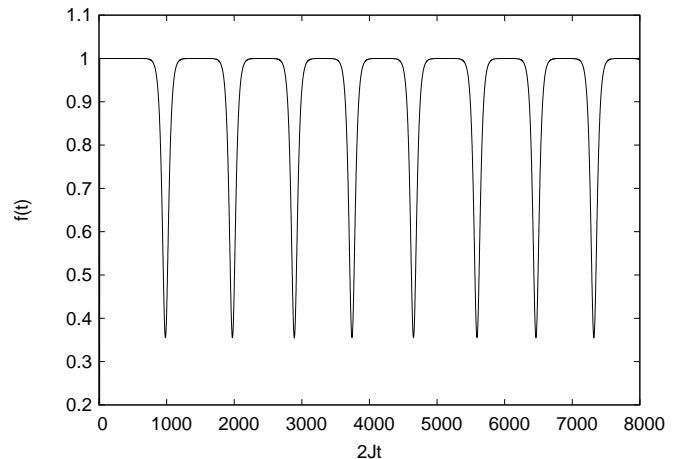


FIG. 4: Fraction of the initial state $f(t)$ in the state of the lattice plotted as a function of time. Here the parameters are $L = 32$, $\Lambda = 0.48$ and $p = \pi$.

The pulsating behavior also manifests in the fraction of the initial state $\psi_l(0)$ remaining in the state of the lattice at a given time,

$$f(t) = \left| \sum_l \psi_l^*(0) \psi_l(t) \right|^2. \quad (27)$$

In Fig. 4 we plot the overlap, $f(t)$, as a function of time for the same parameters as in Fig. 2. It is revealed that the instability drives the system far from, and subsequently brings it back to, the original unstable steady state, and the process repeats. Each dip in the plot represents formation of a pulse during the course of time. It is also noted that the quantity $f(t)$ does not vanish all the way to zero, indicating that the pulsed state is not orthogonal to the initial steady state. Furthermore, a closer inspection of this plot shows that the subsequent peaking events are not strictly periodic; the interval between the dips varies slightly, implying a quasi-periodic phenomenon.

By analyzing data of this kind a number of observations emerge. First, in contradiction to the common belief that the instability may develop into an irregular dynamics, here it causes the atoms to pile up in a single-peaked distribution of the site populations $|\psi_l|^2$. Furthermore, upon continued time evolution, the system returns very close to the initial unstable state, again pulsates to a peak, and so on. We have nearly periodic peaking and recurrences to the unstable initial state. Second, for the initial flow state $p \neq \pi$, the pulse also moves with a velocity that turns out to be close to the group velocity of the carrier wave, $v_g = 2J \sin p$. Third, the peak may occur at any lattice site. It is the random noise that seeds the position of the peak. This is in accordance with translational invariance of the lattice: A lattice-translated pulsed solution is also a solution of the DNLSE, and there is no preferred lattice site for the occurrence of the pulse. Fourth, for weak initial noise the dependence of the pulsation phenomena on the initial noise is otherwise weak. For instance, even if the timing of the first pulse depends logarithmically on the noise amplitude and the spacing of the subsequent peaks is also affected, the dominant time scale is evidently the time scale of the instability from Eq. (25). In Fig. 4 the peak spacing equals approximately $10 \tau_q$.

B. Multiple unstable modes

For a lattice with a large number of sites the one-peak condition (26) is highly impractical because the interaction strength Λ needs to be extremely small and the pulse revival period is correspondingly long. For instance, the shortest possible time scale for the dynamical instability in the one-peak case, τ , is determined from Eqs. (26) and (25) as $2J\tau = L^2 / (2\sqrt{3}\pi^2 |\cos p|) \propto L^2$.

On the other hand, the condition that exactly Q modes are unstable is obtained from Eq. (26) in the form

$$Q^2 |\cos p| \frac{\pi^2}{L} < \Lambda \leq (Q+1)^2 |\cos p| \frac{\pi^2}{L}. \quad (28)$$

For reasonable interaction strengths there might be more than one unstable mode. Figure 5 is a typical representative of the dynamics of the BEC with multiple unstable modes. Here we take $N = 128$, $\Lambda = 2.0$, and $p = \pi$. Each bright spot represents a pulse. As before, the right edge of the plot wraps around to the left edge by virtue of the periodic boundary conditions. Equation (28) gives five unstable modes, while most of the time we see three or four pulses in this example. However, these pulses are not independent. Presumably because of nonlinear mode-mode interaction, they move around, join and split as they collapse and revive.

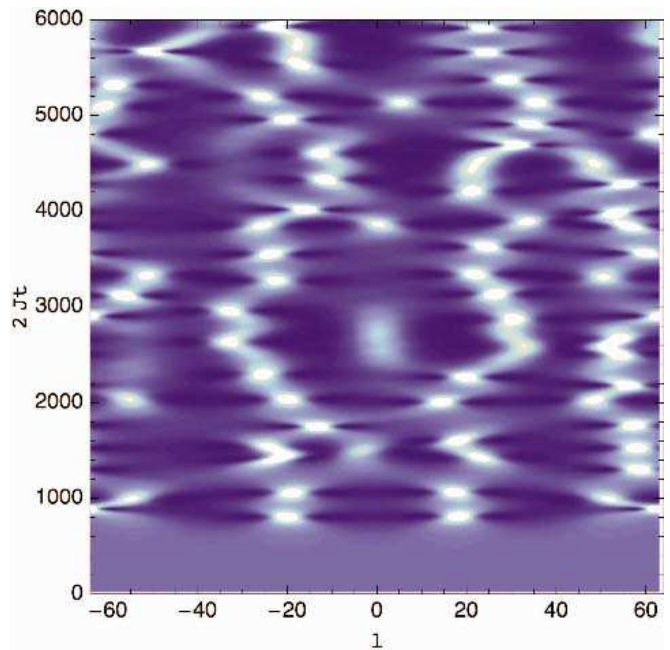


FIG. 5: (Color online) Density plot of the populations $|\psi_l|^2$ in the case where there are four unstable modes. The parameters are $L = 128$, $\Lambda = 2.0$, and $p = \pi$. Lighter shading represents higher site populations.

C. Evolution in Fourier space

The recurrences observed in the peaking events in the DNLSE resemble the energy recurrences in the Fermi-Pasta-Ulam (FPU) problem [35]. The FPU model deals with the evolution of a lattice chain with nonlinear interactions between the nearest-neighbor atoms when initially a single low-energy mode is excited. For a time scale much longer than the time period of the normal modes, the energy is well localized to the given excited mode, while the amplitudes of the higher-energy modes decay exponentially as a function of the energy difference from the initially excited mode. For a longer time scale it has also been noticed that recurrence of the initial excited mode is possible.

The pulsating behavior of the density distribution of the BEC atoms in the lattice can be viewed as a similar recurrence phenomenon as observed in the FPU model. We have started with a steady state for a given flow quasi-momentum ($p > \pi/2$) and a suitable nonlinear interaction strength to trigger the instability in the system. Ergodicity immediately suggests that the energy initially fed into a single mode should distribute evenly between all Fourier modes. However, the excitation amplitudes of the modes other than the mode corresponding to the initial steady state seems to decay exponentially with the index Q . The energy localization to a few Fourier modes in a nonlinear system has been studied also in other systems [29]. The existence of discrete breathers in a nonlinear lattice system is an example. Recently, energy lo-

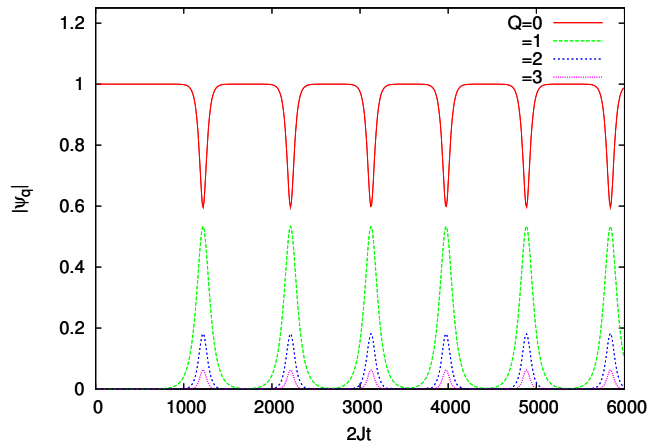


FIG. 6: (Color online) Time evolution of the Fourier modes ψ_q of the lattice. The parameters are $L = 32$, $p = \pi$ and $\Lambda = 0.48$. The mode $Q = 0$ corresponds to the initial steady state while modes $Q = 1, 2, 3 \dots$ are the low-lying excitations. Only the modes with $Q > 0$ are shown.

calization in Fourier space in a so called ‘q-breather’ has been investigated in [36].

Figure 6 shows the time evolution of the Fourier modes ψ_q of DNLSE for the parameters $\Lambda = 0.48$, $N = 32$. Only a few components are seen to be excited, as the amplitudes of the higher-energy modes are suppressed exponentially. The dominant Fourier components are P and $P \pm 1$ which implies that the excitation modes that go unstable should have the indices $Q = \pm 1$ with respect to the initial steady state, as expected.

IV. DOUBLE WELL ANALOGY

In order to explain qualitatively the pulsating behavior of the density distribution of the BEC in the lattice, we study a coupled double-well system. Writing $\psi_{0,1} = |\psi_{0,1}|e^{i\phi_{0,1}}$, the dynamics of such a system can be described by a pair of equations [37]

$$\begin{aligned} \dot{z}(t) &= -\sqrt{1-z^2(t)} \sin \phi(t), \\ \dot{\phi}(t) &= \Lambda z(t) + \frac{z(t)}{\sqrt{1-z^2(t)}} \cos \phi(t), \end{aligned} \quad (29)$$

where $z = |\psi_1|^2 - |\psi_0|^2$ and $\phi = \phi_1 - \phi_0$ are the fractional population imbalance and the relative phase between the two wells. The normalization again is $|\psi_0|^2 + |\psi_1|^2 = 1$. The correct evolution for z and ϕ is obtained from the Hamiltonian

$$H = \frac{\Lambda z^2}{2} - \sqrt{1-z^2} \cos \phi \quad (30)$$

by regarding these quantities as canonical conjugates. The Hamiltonian (energy) is a constant of the motion

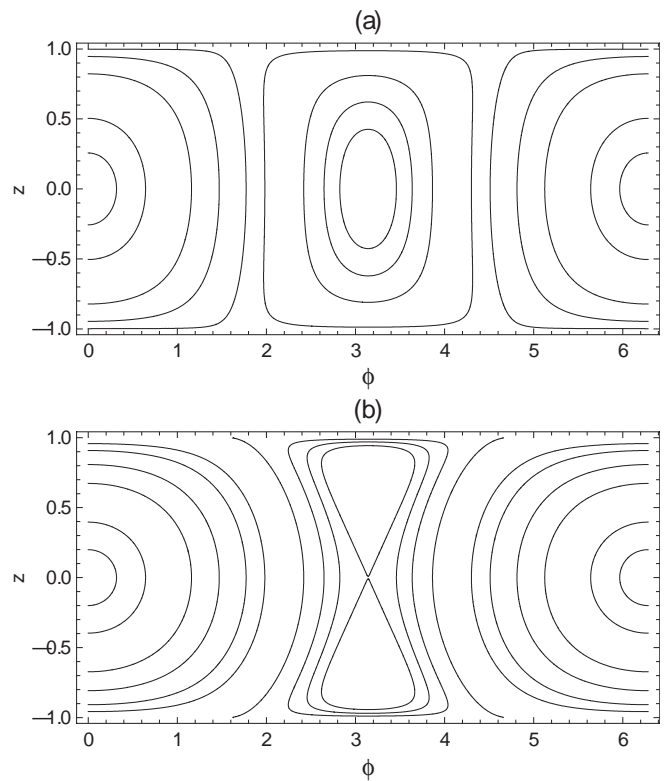


FIG. 7: Representative constant-energy contours of the two-site Hamiltonian (30) in the (ϕ, z) plane for the interaction strengths $\Lambda = 0.5$ (a) and 1.5 (b).

and the double-well system is therefore integrable. The evolution of the system keeps it on a constant-energy contour in the space with z and ϕ as the axes.

By inspection it can be checked that the fixed points of Eq. (29) are $z = 0, \phi = n\pi$, where n is an integer. A potentially unstable steady state in the multiwell system corresponds in the two-well system to the steady state $z = 0, \phi = \pi$. The behavior of the orbits near this equilibrium point can be examined by using linear stability analysis as before. It can be easily verified that the state $(0, \pi)$ is stable for the values $\Lambda \leq 1$, and unstable otherwise.

In Fig. 7 we show constant-energy contours of the two-well system for $\Lambda = 0.5$ (a) and 1.5 (b). We have drawn the ϕ axis from 0 to 2π so that the potentially unstable fixed point $(0, \pi)$ lies at the centers of the panels. For $\Lambda = 0.5$ the potentially unstable steady state is an elliptic fixed point and the time evolution takes the system periodically around this point. At $\Lambda = 1$ the elliptic fixed point bifurcates, and for $\Lambda = 1.5$ there is a homoclinic orbit with the emergence of two symmetric off-centered elliptic fixed points. Thus, starting in the vicinity of what used to be the potentially unstable steady state, the system takes off in an unstable direction along the homoclinic orbit and goes around one of the bifurcated elliptic fixed points.

The double-well system also admits an analytic solu-

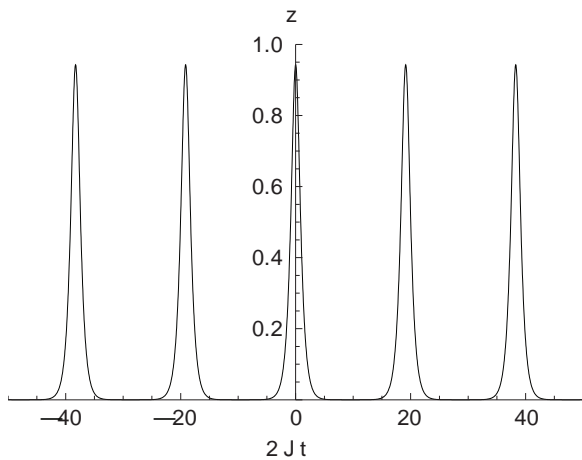


FIG. 8: Time evolution of the population imbalance z given by an exact analytical solution of Eqs. (29) for the parameter $\Lambda = 1.5$ and the value of the Hamiltonian $H = 1.0$.

tion in terms of Jacobian elliptic functions. In Fig. 8 we plot such a solution for $z(t)$ for the parameter $\Lambda = 1.5$ and the conserved value of the Hamiltonian $H = 1.0$. The double-well system is then unstable in linear stability analysis and the energy corresponds to an energy contour close to the homoclinic orbit, see Fig. 6(b). The oscillations in the population imbalance bear a striking resemblance to Fig. 4 with the plot of the overlap in the multiwell lattice, and may be viewed as an analogue of the pulsating instability.

We have presented two different views on the pulsating instability in the two-site system, energy contours and time evolution of the population imbalance, but they describe the same physics. The dynamically unstable system performs periodic oscillation where the system repeatedly recedes far away from the unstable state and subsequently returns.

The multisite system basically shares the behavior of the two-site system in a multi-dimensional phase space: Starting from random noise in the neighborhood of an unstable steady state, it evolves away from, and returns to, the initial state, and the process then repeats. These periodic recurrences occur in a $2L$ -dimensional phase space on a constant-energy surface in full analogy with the two-site system. The two-site system is strictly periodic since there is no motion out of the constant-energy surface, a one-dimensional curve. However, in the multiwell case the dimension of the constant-energy surface is $2L - 1$. Our pulsating instability strongly suggests that the multiwell system stays close to the homoclinic orbit while it evolves. However, depending on the initial noise it still has a large state space to explore, and the motion may deviate slightly from the homoclinic orbit. Upon looping around one of the stable fixed points, the multisite system therefore does not have to return to exactly where it started from. This might account for the slight variations in the period of the pulsations.

In short, we attribute the pulsating dynamics in the multiwell system to a remnant of integrability. The multiwell system evolves along a similar homoclinic orbit that exists in a two-well system, and the motion away from the homoclinic orbit remains bounded.

V. TRUNCATED WIGNER APPROXIMATION

The GPE can constitute a very accurate modeling of a weakly interacting BEC. In Secs. II–IV we discussed the dynamics of a BEC within the classical mean-field theory, including double-well and multi-well systems. We know in the case of double-well systems, however, that when the tunneling barrier becomes large, quantum and thermal fluctuations can considerably influence the atom dynamics [38]. Similarly, in optical lattices the kinetic energy is represented by the hopping of the atoms between adjacent lattice sites, and the hopping amplitude can be significantly reduced in deep lattices. Quantum correlations and fluctuations are a matter of balance between atom-atom interactions and hopping, and may be correspondingly enhanced. In the following we include quantum fluctuations in the dynamics in a lattice using a stochastic phase space method, the truncated Wigner approximation (TWA).

TWA was introduced for multi-mode dynamics in nonlinear optics [22]. Details how to implement TWA in different atomic BEC systems may be found, e.g., in Refs. [23, 24, 25, 26], studies of zero- and finite-temperature nonequilibrium dynamics in 1D lattice systems are documented in Refs [15, 19, 26, 39, 40, 41], and the effects of dynamical instabilities in lattices have been explicitly addressed in Refs. [15, 19, 39]. In the TWA one neglects the third-order derivatives in the generalized Fokker-Planck like equation for a Wigner distribution function [43]. This permits a nonlinear stochastic differential equation for a classical field that represents the quantum field. Here the equation is just the DNLS.

In our present case of TWA quantum fluctuations and correlations enter only through the stochastic initial state of the classical field. Our emphasis on quantum fluctuations is different from typical finite-temperature dominated TWA approaches in higher dimensions [42]. In an attempt to capture quantum mechanics as accurately as practicable, we therefore pick the initial states of the wave function using the Bogoliubov approximation.

In our numerical simulations we consider a stable stationary superfluid flow that is instantaneously, at $t = 0$, rendered dynamically unstable by changing atom-atom interactions. We investigate the effect of quantum fluctuations by considering two different types of initial states: a noninteracting BEC with all atoms in the same one-particle state, and an interacting system in which the atom-atom interactions force fraction of the atoms out of the condensate. We first generate a stochastic initial state $\psi_l^W(t = 0)$ accordingly, then the TWA dynamics

follows from the DNLSSE

$$i\frac{\partial}{\partial t}\psi_l^W = -J(\psi_{l+1}^W + \psi_{l-1}^W) + \chi|\psi_l^W|^2\psi_l^W. \quad (31)$$

This process is repeated for a number of initial states. Two types of results are of interest: Individual trajectories $\psi_l^W(t)$ represent the outcomes of individual experiments, and appropriate averages over the collection of trajectories are used to calculate pertinent quantum expectation values. The present TWA formalism is very similar to the one used in Refs. [15, 26, 40], except that in each TWA realization we fix the total atom number [44].

A. Initial state

In order to describe the generation of the stochastic initial states for the TWA dynamics we begin with the quantum version of the Bogoliubov approximation. We again consider the stationary solution for a moving plane wave as in Eqs. (8) and (11). The fluctuations around the stationary solution are governed by the decomposition of the atom field operator

$$\hat{\psi}_l(t) = \psi_l^0(t)\hat{\alpha}_0 + \delta\hat{\psi}_l(t), \quad (32)$$

where the total number of condensate atoms,

$$N_c = \langle \hat{\alpha}_0^\dagger \hat{\alpha}_0 \rangle,$$

is assumed much larger than one and $\delta\hat{\psi}_l(t)$ is supposedly “small.” Heretofore we make a difference between total number of atoms N , number of condensate atoms N_c , and number of noncondensate atoms N_n . Analogously to our earlier classical Bogoliubov treatment, the fluctuation part of the atom field operator, $\delta\hat{\psi}_l(t)$, can be written in terms of quasiparticle operators $\hat{\alpha}_q$ and $\hat{\alpha}_q^\dagger$ as

$$\delta\hat{\psi}_l(t) = \frac{1}{\sqrt{L}} \sum_{q \neq 0} (u_q \hat{\alpha}_q e^{i(p+q)l - i\Omega_q t} + v_q^* \hat{\alpha}_q^\dagger e^{i(p-q)l + i\Omega_q^* t}). \quad (33)$$

Within the Bogoliubov approximation the quasiparticles make a bosonic ideal gas, or alternatively, the operators $\hat{\alpha}_q$ may be viewed as the lowering operators for a collection of independent harmonic oscillators. The normal mode frequency Ω_q and the quasiparticle amplitudes u_q , and v_q are given by Eqs. (16), (18), and (19); only the excitation modes with positive normalization are used. The unit normalizations for both the unperturbed plane wave ψ_l^0 and the amplitudes of the excitation modes u_q , v_q were fixed earlier so that these quantities work as given also in the present quantum version of Bogoliubov theory.

The expectation value of the number of non-condensate atoms in the Bogoliubov theory is

$$\bar{N}_n = \sum_q (|u_q|^2 + |v_q|^2) \langle \hat{\alpha}_q^\dagger \hat{\alpha}_q \rangle + \sum_q |v_q|^2, \quad (34)$$

with

$$\langle \hat{\alpha}_q^\dagger \hat{\alpha}_q \rangle = [e^{\Omega_q/k_B T} - 1]^{-1}. \quad (35)$$

At $T = 0$ we have $\langle \hat{\alpha}_q^\dagger \hat{\alpha}_q \rangle = 0$, and the non-condensate atom number is simply

$$\bar{N}_n = \sum_q |v_q|^2. \quad (36)$$

In order to construct the initial state of the lattice for TWA evolution we replace the quantum operators ($\hat{\alpha}_q, \hat{\alpha}_q^\dagger$) in Eq. (33) by complex stochastic variables (α_q, α_q^*) obtained by sampling the corresponding Wigner distribution function. Our formalism follows Ref. [26], except that here we fix the total atom number [44]. The Wigner function at $T = 0$ is [43]

$$W(\alpha_q, \alpha_q^*) = \frac{2}{\pi} \exp[-2|\alpha_q|^2]. \quad (37)$$

The function $W(\alpha_q, \alpha_q^*)$ is a Gaussian and we easily find the average number $\langle \alpha_q^* \alpha_q \rangle_W = \frac{1}{2}$ of excitations in each mode q owing to quantum noise. Each unoccupied excitation mode exhibits uncorrelated Gaussian noise, distributed over the plane wave basis, and normalized to an average of a half an excitation quantum per mode. The attendant atoms provide seeding for scattering events in the TWA dynamics. However, Wigner functions correspond to symmetrically ordered expectation values of functions of the operators $\hat{\alpha}_q$ and $\hat{\alpha}_q^\dagger$, and in the end the expectations values $\langle \alpha_q^* \alpha_q \rangle_W = \frac{1}{2}$ need to be subtracted to obtain normally-ordered quantum averages. For each stochastic realization, the number of non-condensate atoms therefore reads

$$N_n = \sum_q (|u_q|^2 + |v_q|^2) (\alpha_q^* \alpha_q - \frac{1}{2}) + \sum_q |v_q|^2. \quad (38)$$

This may fluctuate about the mean value $\bar{N}_n = \sum_q |v_q|^2$ for each realization, but correctly averages to \bar{N}_n .

Since the total atom number N is fixed, the number of condensate atoms in each individual run is given by

$$N_c = N - N_n, \quad (39)$$

which also fluctuates around the mean value $\bar{N}_c = N - \bar{N}_n$. In the initial state for each realization we then set

$$\alpha_0 = \sqrt{N_c + 1/2}, \quad (40)$$

so that, in the place of Eq. (32), we have the initial state for the TWA method

$$\psi_l^W(0) = \psi_l^0(0)\alpha_0 + \frac{1}{\sqrt{L}} \sum_{q \neq 0} (u_q \alpha_q e^{i(p+q)l} + v_q^* \alpha_q^* e^{i(p-q)l}), \quad (41)$$

where α_q and α_q^* are stochastic variables in each realization of the TWA. Note that, even though we consider

a uniform system with a plane wave phonon basis and uncorrelated noise in the initial phonon modes, the fixing of the total atom number introduces long wavelength correlations in the system between the condensate mode and the excited quasiparticle modes [44].

Based on the Bogoliubov results it is interesting to estimate when the classical description of the condensate dynamics from the DNLS, as in Eq. (5), approaches the quantum results, as per the TWA. For instance, if the ratio of non-condensate particles to condensate particles in the initial state is large, one may expect the classical DNLS to provide an especially poor approximation. Now, the expression (19) for the amplitudes v_q shows that the interaction strength enters through the dimensionless parameter χ/J . By virtue of our normalizations, the interaction parameter χ , Eq. (7), is proportional to the number of atoms. If the number of atoms is increased while adjusting the strength of the atom-atom interactions in such a way that χ/J is held constant, the number of noncondensate atoms remains constant and the ratio of non-condensate particles to condensate particles in the initial state is reduced. We expect the error in DNLS correspondingly become smaller [15]. In fact, even if the non-condensate population in the initial state vanishes, the relative contribution of the vacuum Wigner noise is reduced when the condensate population is increased, and we again expect the error in DNLS to be reduced.

The potential instability, however, adds a new element to the picture. Namely, for the consistency of our present development the excitation modes must be normalized to $|u_q|^2 - |v_q|^2 = 1$, whereas for an unstable mode necessarily $|u_q|^2 - |v_q|^2 = 0$ holds true. This means that when the point of dynamical instability is approached continuously, for some mode q the amplitudes diverge, $|u_q| \rightarrow \infty$ and $|v_q| \rightarrow \infty$. By Eq. (36) the number of noncondensate atoms also diverges, $\bar{N}_n \rightarrow \infty$. At the point of instability steady-state quantum fluctuations diverge, according to the Bogoliubov approximation. The Bogoliubov method is based on the assumption of *small* fluctuations so that it in itself fails for an unstable system, but it is clear that the onset of instability is associated with large quantum fluctuations.

While the asymptotic results are easy to infer, only a detailed analysis can tell what the number of noncondensate atoms is in a specific situation. Figure 9 shows the number of noncondensate atoms N_n as a function of the interaction parameter Λ for the number of lattice sites $L = 32$. Both the generally very small number of noncondensate atoms for weak interactions and the divergence at the onset of instability $\Lambda = 0.308 \simeq \pi^2/L$ are evident.

B. Numerical realization

We study the non-equilibrium quantum dynamics of a BEC within TWA. We consider a BEC in a lattice that

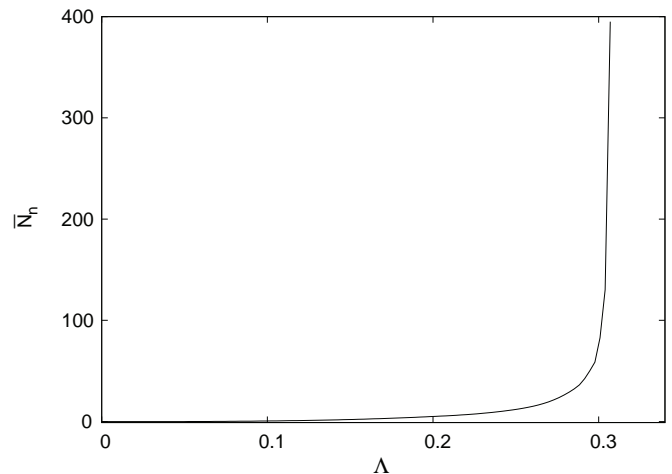


FIG. 9: Number of noncondensate atoms \bar{N}_n given by Eq. (36) as a function of the scaled interaction strength Λ within Bogoliubov approximation for $L = 32$. Note that the critical interaction strength at the onset of the instability is 0.308.

is initially in a stable steady flow state. This is crucial for the validity of the Bogoliubov approximation for the initial state as well as for the generation of the stochastic initial noise in the TWA. A stable state of the atomic gas can be experimentally driven to a dynamically unstable state, for instance, by starting with a moving lattice with the quasimomentum of the atoms $p < \pi/2$ and accelerating the lattice so that the momentum satisfies $p > \pi/2$. In our examples, though, we envisage suddenly modifying atom-atom interactions. Henceforth we always have the number of lattice sites $L = 32$ and the initial flow state with $p = \pi$. We perform the simulations for two different types of initial states: noninteracting atoms with all atoms in the condensate, and an interacting state with a nonzero condensate depletion. As to the interacting initial state, we select the dimensionless interaction strength $\Lambda = \chi/2J = 0.284$. For this value the average noncondensate atom number is $\bar{N}_n \simeq 30$ whereas the critical value of Λ at the onset of the instability is 0.308, as per Fig. 9. In all cases considered here, the initial depletion \bar{N}_n/N is less than 10%, and the Bogoliubov approximation for the initial state is presumed accurate. At the beginning of the time evolution the atom-atom interactions are turned up instantaneously to the dynamically unstable value of $\Lambda = 0.48$. We investigate the effect of quantum fluctuations by varying the total atom number N and the atomic interaction strength g (Eq. (7)) so that the interaction parameters χ and Λ (and the chemical potential) remain constant.

For each individual realization of the time evolution of the ensemble of the Wigner distributed wave functions we sample the initial state as explained in the previous Section V B. The random numbers (α_q, α_q^*) are obtained using the Box-Mueller algorithm [33]. As before, we integrate the dynamical equations (31) using the FFT split-step method [34]. Depending on the task at hand, we

either study the individual trajectories $\psi_l^W(t)$, or averages over a number of trajectories.

It should be noted that our process contains an uncontrolled approximation. There are some indications [15, 26, 45, 46] that time evolution as prescribed by TWA could become exact in the asymptotic limit $N \rightarrow \infty$ with a fixed χ , but even if this were the case, the asymptotic limit per se does not tell how good the results are for given values of the parameters. For instance, we do not know how long the TWA time integration remains valid. This question should be studied fully quantum mechanically, but at the present time we do not know of any framework to address the issue. How would one describe the modulational instability of a classical nonlinear system ab initio using linear quantum mechanics, which by definition prescribes a stable evolution of any initial state? Moreover, in a classical instability the translation invariance of the state of the lattice is broken, but unitary time evolution from quantum mechanics will not spontaneously break any symmetry of the Hamiltonian. For the time being we rely on the practical observation from working with the TWA method that it usually signals its own demise. Typically, upon integrating long enough, each individual trajectory seemingly loses any relation to the initial state. In our computations we have not encountered a situation of this kind.

C. Results

Since the Wigner functions govern symmetrically ordered expectation values, we need certain transformations to calculate the ordinary normally ordered expectation values from the simulation data [26, 40]. Here we only consider the lowest-energy band in the tight-binding approximation, so normally ordering the operator expectation values is straightforward. According to Ref. [26], we have the atom number in a lattice site

$$n_l = \langle \psi_l^* \psi_l \rangle_W - \frac{1}{2}, \quad (42)$$

with the corresponding fluctuations

$$\Delta n_l = \sqrt{\langle (\psi_l^* \psi_l)^2 \rangle_W - \langle \psi_l^* \psi_l \rangle_W^2 - \frac{1}{4}}. \quad (43)$$

The overlap of the field amplitudes $\psi_l(0)$ and $\psi_l(t)$, which is a measure of the revival of the pulse, is given by

$$f^W(t) = \langle |\sum_l \psi_l^*(t) \psi_l(0)|^2 \rangle_W. \quad (44)$$

In Fig. 10 we show typical single-trajectory results for the overlaps $f(t)$ for different values of the atom-atom interactions g and the total atom number N . All different cases have the initial interaction parameter $\Lambda = Ng/(2J) = 0.284$ that is instantaneously changed to $\Lambda = 0.48$, but the values of N and g are varied individually so that the total number of atoms is (a) $N = 10^6$, (b) $N = 10^4$, (c) $N = 10^3$, and (d) $N = 500$.

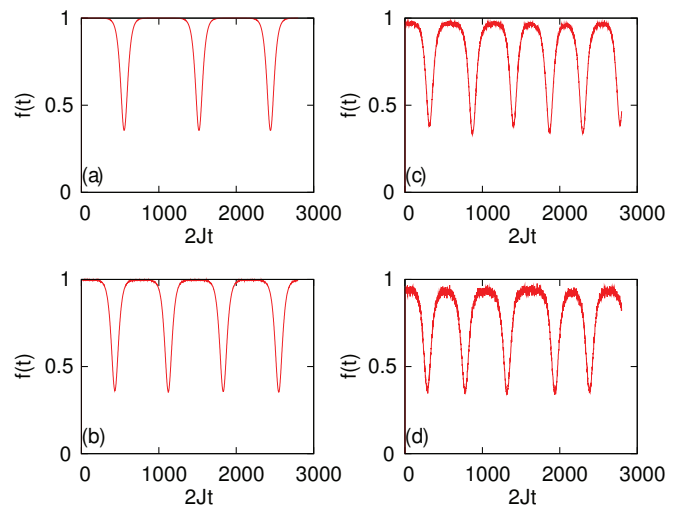


FIG. 10: (Color online) Overlap of a single stochastic realization with the initial state as a function of time sampled from the Wigner distribution for a fixed chemical potential with different atom numbers (a) $N = 10^6$, (b) $N = 10^4$, (c) $N = 10^3$ and (d) $N = 500$. The initial state is interacting with $\bar{N}_n = 30$. The parameters of the simulation are $\Lambda = 0.48$, $L = 32$, and $p = \pi$. There is no significant damping in the oscillation even if the noncondensate noise is substantial.

The number of noncondensate atoms in the Bogoliubov approximation does not change whenever we vary \bar{N}_c and g for a fixed value of $\bar{N}_c g$. For a smaller total number of atoms N , the noncondensate atom fraction \bar{N}_n/N in the initial state and the coupling constant g are larger and, consequently, quantum effects are stronger. Each plot in Fig. 10 clearly shows the pulsating instability without any noticeable damping. Quantum fluctuations and the initial noncondensate population act as a seed for the scattering processes taking atoms out of the ground state. The period of the pulsating instability depends on the interaction coefficient g , albeit not dramatically; the larger the value of g (corresponding to the smaller value of N), the shorter the period of oscillation, since higher scattering rate leads to a faster ground state depletion and, consequently, a shorter oscillation period.

Figure 11 represents an ensemble average of the overlap $f^W(t)$ sampled over 400 trajectories for the total number of atoms (a) $N = 10^4$, (b) $N = 10^3$, (c) $N = 500$ and (d) $N = 300$ for the interacting (solid curve) and the noninteracting (dashed curve) initial states. In all cases the final value of the interaction parameter is again $\Lambda = 0.48$ ($\propto Ng$), but the nonlinearity g and the total atom number N are different.

While the almost undamped quasiperiodic behavior is seen in individual stochastic realizations, the quantum mechanical ensemble averages of the wave function revival become progressively weaker when the effective interaction strength is increased. This is because the shape and the timing of the pulsations in each realization change due to quantum fluctuations. Enhanced quan-

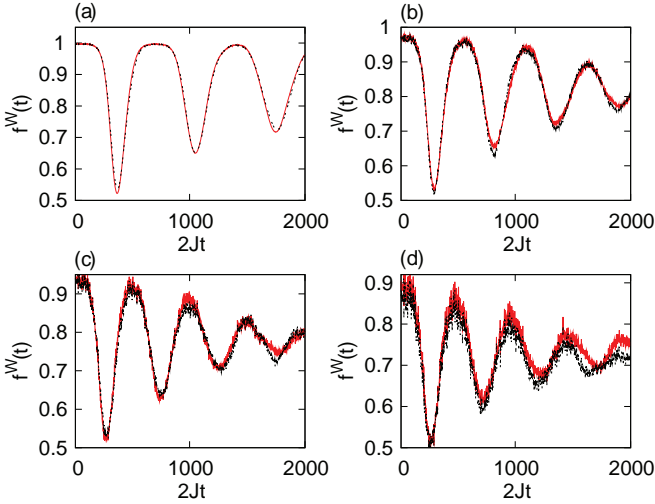


FIG. 11: (Color online) Comparison of the ensemble average of the overlap of the state of the lattice sampled over 400 realizations for the initial number of non-condensate atoms $\bar{N}_n = 0$ (solid line) and $\bar{N}_n = 30$ (dashed line), and for the total number of atoms (a) $N = 10^4$, (b) $N = 10^3$, (c) $N = 500$ and (d) $N = 300$. The parameters of the simulations are $\Lambda = 0.48$, $L = 32$, and $p = \pi$. The two different initial states represent similar time evolution when the total atom number is large. However, the curves start deviating as the number of atoms is reduced.

tum fluctuations for smaller N (and larger g) are clearly observable in increased damping rates. For the interacting initial state, the initial noncondensate atom fraction only if the total atom number is small, and so the results for the noninteracting and interacting initial states differ significantly only for small total atom numbers. Figure 12 represents a comparison of the overlaps in a typical single realization and in an ensemble average for the large atom number $N = 10^6$, and with the interacting initial state. The other parameters of the simulations are same as in Fig. 11.

Similar damping is also observed in the atom number fluctuations at a fixed site, say, center of the lattice. In Fig. 13 we show ensemble averages of the atom number fluctuations $\Delta n/\sqrt{n}$ for the total number of the atoms (a) $N = 10^4$, (b) $N = 10^3$, (c) $N = 500$ and (d) $N = 300$ and for the interacting initial state. The parameters of the simulations are as before. The pulsating instability causes strongly super-Poissonian atom number fluctuations at any fixed lattice site.

The main focus in this work is to estimate the inherent quantum effects on the pulsation phenomenon of the BEC in an optical lattice. We have found that quantum fluctuations have an effect on the collapse and revival of the pulse. In the case of a single realization the revival is very robust and repeats over a long time. The ensemble averages of the overlap of the wave function revival display a recognizable damping behavior due to quantum

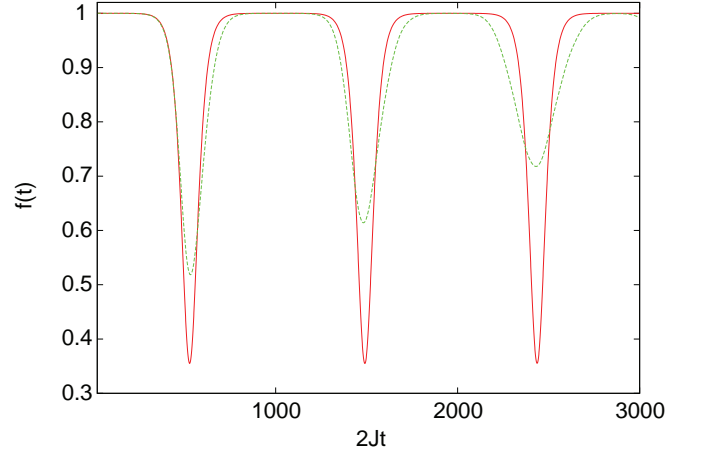


FIG. 12: (Color online) Comparison of the overlaps in a typical single realization (solid line) versus an ensemble average sampled over 400 realizations (dashed line) with the initial interacting state for $\bar{N}_n = 30$ and $N = 10^6$. The parameters of the simulations are $\Lambda = 0.48$, $L = 32$ and $p = \pi$.

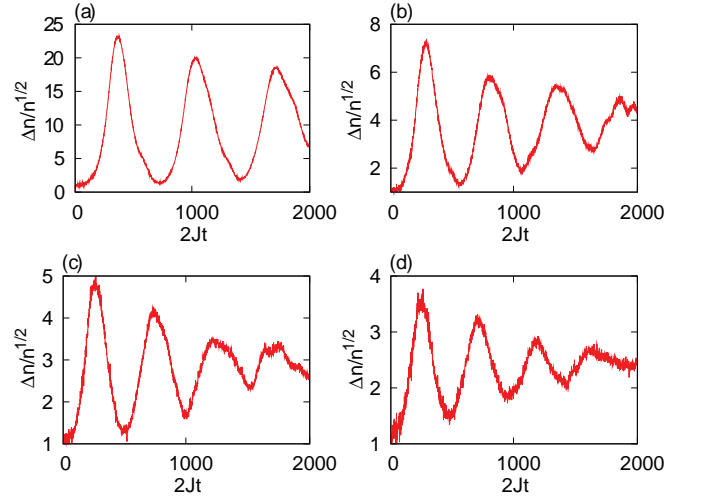


FIG. 13: (Color online) Atom number fluctuations in the central lattice site as a function of time sampled over 400 realizations for the total numbers of particles (a) $N = 10^4$, (b) $N = 10^3$, (c) $N = 500$ and (d) $N = 300$ with $N_n = 30$. We use the interacting initial state.

fluctuations. We have also found that the damping rate is increased if the initial state is depleted with a nonnegligible noncondensate fraction.

The TWA also provides for computing of quantities that are affected by quantum fluctuations and could be readily measurable, but may be very difficult to extract from the full quantum solution of the problem if it were on hand. Parameters for the shape of the pulse, obscured in quantum mechanics by averaging over the random time and position of the pulse, are an example. In Fig. 14 we show the amplitude for the first pulse in the pulsating instability as a function of the total number of atoms

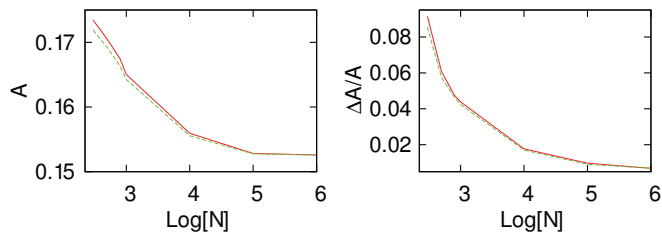


FIG. 14: (Color online) Ensemble average of the amplitude (left) of the first peak and its fluctuations (right) during pulsation as a function of the total number of atoms, N , for a fixed chemical potential for interacting (solid line) and non-interacting (dashed line) initial states. The parameters of the simulation are same as in Fig. 11. The amplitude reaches the classical value for higher atom numbers. Quantum noise increases the amplitude and the fluctuations of the amplitude for small atom numbers.

(for a fixed nonlinearity, as before), and its fluctuations. These are averaged over 400 realizations, both for the interacting (solid curve) and the noninteracting (dashed curve) initial states. The parameters of the simulations are the same as in Fig. 11.

The pulse amplitude approaches a classical value that may be obtained from the GPE in the limit of weak quantum fluctuations (here corresponding to large N and small g). However, both the amplitude of the atom pulse and the amplitude fluctuations grow when the atom number becomes small and quantum fluctuations become more dominant. Similarly to the case of the overlap revival, the distinction between the two initial states is apparent only when the noncondensate fraction is nonnegligible.

VI. CONCLUDING REMARKS

In this paper we have presented new insights into the unstable dynamics of the BEC in an optical lattice in the limit of weak atom-atom interactions, with quantum fluctuations included. The common belief is that the flow of the dynamically unstable BEC in an optical lattice would be erratic, or lead to the formation of stable solitons. Here we move a step further and show that, in classical mean-field theory, the instability may also trigger a quasi-periodic pulsation in the atom density distribution if the atom-atom interactions are weak. The requirement

that linear stability analysis finds a single unstable mode gives the scale for the ‘weak’ nonlinearity and the ensuing pulsating phenomena.

A qualitative argument has been put forward to explain the pulsating behavior of the dynamics by comparing the lattice system with the integrable double-well system. In the case of two wells the unstable mode leads to a non-trivial dynamics in the population imbalance such that an infinitesimal noise could produce a large-amplitude collective oscillation of the atoms between the wells. We surmise that the pulsating instability is a remnant of the integrability as manifest in the two-well system.

We incorporate quantum fluctuations using stochastic phase-space methods. We use the Bogoliubov approximation to generate the initial state for the time evolution of the system. A sequence of the stochastic fields obtained in this way are then used to calculate expectation values of the observables. We also compare the single realization results with the ensemble averages. Generally speaking, the pulsating behavior survives in the face of quantum fluctuations. It is observed that the quasiperiodic behavior in the time dynamics can still be seen in single realizations. However, the quantum averages show that the revivals of the pulses tend to get washed out as the atom number gets smaller while the chemical potential is held constant.

For experimental realizations, the flow states $p \approx \pi$ near the Brillouin zone boundary can be prepared by accelerating the lattice [8]. Alternatively, by exploiting the symmetry of the DNLS, for every solution $\psi_l(t)$ with the given interaction parameter Λ there is a solution $(-1)^l \psi_l^*(t)$ for $-\Lambda$. That means the state for $p = \pi$ in the repulsive case is equivalent to the state for $p = 0$ in the attractive case. Manipulation of the sign of the interactions gives much additional leeway for the experiments. However, given that the pulsating phenomenon only occurs in the limit of weak nonlinearity, the corresponding time scales for the pulsation can be very long and pose severe technical challenges.

Acknowledgments

We acknowledge financial support from NSF (PHY-0750668) and EPSRC.

[1] O. Morsch and M. Oberthaler, *Rev. Mod. Phys.* **78**, 179 (2006).
 [2] C. Pethick and H. Smith, *Bose-Einstein condensation in dilute gases* (Cambridge University Press, Cambridge, 2002).
 [3] S. Burger, F.S. Cataliotti, C. Fort, F. Minardi, M. Inguscio, M.L. Chiofalo, and M.P. Tosi, *Phys. Rev. Lett.* **86**, 4447 (2001).

[4] B. Wu and Q. Niu, *Phys. Rev. A* **64**, 061603(R) (2001).
 [5] A. Smerzi, A. Trombettoni, P.G. Kevrekidis, and A.R. Bishop, *Phys. Rev. Lett.* **89**, 170402 (2002).
 [6] F.S. Cataliotti, L. Fallani, F. Ferlaino, C. Fort, P. Maddaloni, and M. Inguscio, *New J. Phys.* **5**, 71 (2003).
 [7] M. Cristiani, O. Morsch, M. Malossi, M. Jona-Lasinio, M. Anderlini, E. Courtade, and E. Arimondo, *Opt. Express* **12**, 4 (2004).

- [8] L. Fallani, L. De Sarlo, J.E. Lye, M. Modugno, R. Saers, C. Fort, and M. Inguscio, *Phys. Rev. Lett.* **93**, 140406 (2004).
- [9] L. De Sarlo, L. Fallani, J.E. Lye, M. Modugno, R. Saers, C. Fort, and M. Inguscio, *Phys. Rev. A* **72**, 013603 (2005).
- [10] B. Wu and Q. Niu, *New J. Phys.* **5**, 104 (2003).
- [11] A. Trombettoni and A. Smerzi, *Phys. Rev. Lett.* **86**, 2353 (2001).
- [12] C.D. Fertig, K.M. O'Hara, J.H. Huckans, S.L. Rolston, W.D. Phillips, and J.V. Porto, *Phys. Rev. Lett.* **94**, 120403 (2005).
- [13] Y. Zheng, M. Kostrun, and J. Javanainen, *Phys. Rev. Lett.* **93**, 230401 (2004).
- [14] M. Modugno, C. Tozzo, and F. Dalfovo, *Phys. Rev. A* **70**, 043625 (2004).
- [15] J. Ruostekoski and L. Isella, *Phys. Rev. Lett.* **95**, 110403 (2005).
- [16] J. Gea-Banacloche, A.M. Rey, G. Pupillo, C.J. Williams, and C.W. Clark, *Phys. Rev. A* **73**, 013605 (2006).
- [17] J. Ruostekoski and Z. Dutton, *Phys. Rev. A* **76**, 063607 (2007).
- [18] G. Barontini and M. Modugno, *Phys. Rev. A* **76**, 041601(R) (2007).
- [19] A. J. Ferris, M. J. Davis, R. W. Geursen, P. B. Blakie, and A. C. Wilson *Phys. Rev. A* **77**, 012712 (2008).
- [20] U. Shrestha, M. Kostrun, and J. Javanainen, *Phys. Rev. Lett* **101**, 070406 (2008).
- [21] A. Polkovnikov, E. Altman, E. Demler, B. Halperin, and M.D. Lukin, *Phys. Rev. A* **71**, 063613 (2005).
- [22] P.D. Drummond and A.D. Hardman, *Europhys. Lett.* **21**, 279 (1993).
- [23] M.J. Steel, M.K. Olsen, L.I. Plimak, P.D. Drummond, S.M. Tan, M.J. Collett, D.F. Walls, and R. Graham, *Phys. Rev. A* **58**, 4824 (1998).
- [24] A. Sinatra, C. Lobo, and Y. Castin, *J. Phys. B* **35**, 3599 (2002).
- [25] C. W. Gardiner, J. R. Anglin, and T. I. A. Fudge, *J. Phys. B* **35**, 1555 (2002).
- [26] L. Isella and J. Ruostekoski, *Phys. Rev. A* **74**, 063625 (2006).
- [27] L. P. Pitaevskii, *Sov. Phys. JETP* **13**, 451 (1961); E. P. Gross, *J. Math. Phys.* **4**, 195 (1963).
- [28] D. N. Christodoulides and R. J. Joseph, *Opt. Lett.* **13**, 794 (1998).
- [29] T. Dauxois and M. Peyrard, *Phys. Rev. Lett.* **70**, 3935 (1993); P.J.Y. Louis, E.A. Ostrovskaya, C.M. Savage, and Y.S. Kivshar, *Phys. Rev. A* **67**, 013602 (2003).
- [30] Nail N. Akhmediev and Adrian Ankiewicz, *Solitons Non-linear pulses and beams* (Chapman & Hall, London, 1997).
- [31] J. Javanainen, S. M. Paik, and S. M. Yoo, *Phys. Rev. A* **58**, 580 (1998).
- [32] J. Javanainen and Y. Zheng, *Phys. Rev. A* **63**, 063610 (2001).
- [33] W. P. Press *et al.*, *Numerical Recipes in C* (Cambridge University Press, 1997).
- [34] J. Javanainen and J. Ruostekoski, *J. Phys. A* **39**, L179 (2006).
- [35] E. Fermi, J. Pasta, and S. Ulam, Los Alamos Report **LA-1940** (1955).
- [36] S. Flach, M.V. Ivanchenko, and O.I. Kanakov, *Phys. Rev. Lett.* **95**, 064102 (2005); S. Flach and A. Gorbach, *Chaos* **15**, 015112 (2005).
- [37] S. Raghavan, A. Smerzi, S. Fantoni, and S.R. Shenoy, *Phys. Rev. A* **59**, 620 (1999); A. Smerzi, S. Fantoni, S. Giovanazzi, and S.R. Shenoy, *Phys. Rev. Lett.* **79**, 4950 (1997).
- [38] J. Ruostekoski and D. F. Walls, *Phys. Rev. A* **58**, R50 (1998).
- [39] A. Polkovnikov and D.W. Wang, *Phys. Rev. Lett.* **93**, 070401 (2004).
- [40] L. Isella and J. Ruostekoski, *Phys. Rev. A* **72**, 011601(R) (2005).
- [41] A.K. Tuchman, C. Orzel, A. Polkovnikov, and M.A. Kasevich, *Phys. Rev. A* **74**, 051601(R) (2006).
- [42] R.N. Bisset, M.J. Davis, T.P. Simula, and P.B. Blakie, arXiv:0804.0286.
- [43] C. W. Gardiner and P. Zoller, *Quantum Noise* (Springer, Berlin, 1999).
- [44] A. D. Martin and J. Ruostekoski, unpublished.
- [45] J. Berges and T. Gasenzer, *Phys. Rev. A* **76**, 033604 (2007).
- [46] F. Trimborn, D. Witthaut, and H. J. Korsch, *Phys. Rev. A* **77**, 043631 (2008).